Multiple segment spectacle lenses for myopia control. Part 1: Optics

Hema Radhakrishnan[1]
Carly Siu Yin Lam[2,3]
W. Neil Charman[1]

Author affiliations:
[1] Faculty of Biology, Medicine and Health, University of Manchester, Manchester M60 1QD, UK

[2]Centre for Myopia Research, School of Optometry, The Hong Kong Polytechnic University, Hung Hom, Kowloon, Hong Kong

[3] Centre for Eye and Vision Research (CEVR), Hong Kong SAR, China

Correspondence to:

Dr Hema Radhakrishnan
Reader in Optometry
Division of Pharmacy and Optometry
Faculty of Biology, Medicine and Health
The University of Manchester
Manchester M13 9PL
Email:Hema.Radhakrishnan@manchester.ac.uk

Running title: Multiple segment spectacle lenses for myopia control

Abstract

Purpose: To understand and compare the optics of two multiple-segment (MS) spectacle lenses (Hoya Miyosmart and Essilor Stellest) designed to inhibit myopia progression in children.

Methods: The optics of the two designs are presented, together with geometrical optics-based calculations to understand the impact of the lenses on the optics of the eye. Lenses were evaluated with three techniques: surface images, Twyman-Green interferometry, and focimetry. The carrier lens powers and the spatial distribution, powers and forms of the lenslets were measured.

Results: MS lenses as manufactured were found to match most of the design specifications given by their manufacturers, although some apparent small discrepancies were found. The focimeter-measured power of the lenslets was approximately +3.50 D for the Miyosmart and +4.00 D for the highly-aspheric lenslets of the Stellest design. For both designs of lens, image contrast would be expected to be modestly reduced in the focal planes of the distance-correcting carrier lenses. Images become much more degraded in the combined carrier-lenslet focal plane, due to the generation of multiple laterally-displaced images formed by adjacent lenslets within the effective pupil. The exact effects observed depend on the effective pupil size and its location with respect to the lenslets, and the power and arrangement of the lenslets.

Conclusion: Wear of either of these lenses will produce broadly similar effects on retinal imagery.

Introduction

Over the last few decades, the prevalence of myopia has increased in many parts of the world. This has led to concerns regarding the consequent cost of treatment, increased risk of associated pathology, and loss in quality of life.[1-3] Recently, a new type of spectacle lens, the multiple segment (MS) lens, has been introduced.[4, 5] In such lenses, multiple small (ca 1 mm diameter), positively-powered lenslets are embossed across all or part of the periphery of the anterior surface of a distance correction (the carrier lens). As in several earlier attempts to produce a myopia-controlling spectacle lens,[6, 7] the lenses are designed to act by introducing a myopic defocus in the peripheral retina to achieve myopia control, as indicated by the results of experiments with animals.[8-11]

The earliest design of this type was the MiyoSmart or DIMS (Defocus Incorporated Multiple Segment) lens (Hoya, Tokyo, Japan) in which the small lenslets are arranged in a triangular (honeycomb) pattern, within a hexagonal “annulus”, on the anterior surface of the carrier lens.[5] The central region of the carrier lens around its optical centre is left clear (Figure1a). Normally the visual axis is directed to view through this central clear area. The optics of the lens are outlined in the original patent[12] and by Lam et al.[13,] and have been analysed in much more detail by Jaskulski et al.[14] and Gantes-Nunez et al.[15] Essentially, rays from a distant object point at a field angle such that the rays pass through the lenslet-covered area of the lens in their passage to the pupil of the eye are nominally brought to two foci, the first formed by the basic distance correction the other myopic focus being generated by the combined powers of the distance correction and each embossed lenslet.

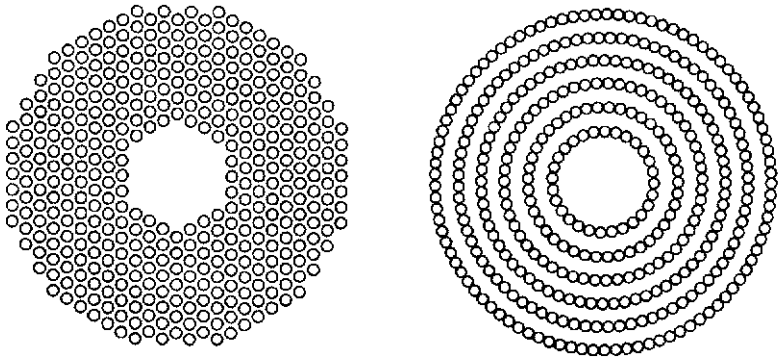

(a) (b)

Figure 1. Schematic arrangement of lenslets in (a) MiyoSmart lenses (Hoya) and (b) Stellest lenses (Essilor). In practice the widths of the clear areas at the centre of both current lenses are about 9 mm.

The same basic Multiple Segment (MS) concept is extended to lenses (Stellest lenses, Essilor, Paris, France) in which the lenslets are arranged in a series of concentric circles surrounding the central clear area, rather than being distributed in a triangular lattice (see Figure1b).[4, 16-18] Further, rather than being spherical, the surfaces of the lenslets are either slightly or highly aspheric (SALs or HALs). It is argued that this asphericisation results in the myopic focus of the lenslets being extended in depth to create a “volume of myopic focus” rather than a single plane of myopic defocus, the concept being termed HALT (Highly Aspheric Lenslet Target) technology, by the manufacturers. This extended focus effect is similar to that produced by aspheric designs of simultaneous-image presbyopic contact lenses. As with the earlier MiyoSmart lenses,[19, 20] short-term tests with children showed that acuity and contrast sensitivity when looking through the lenslet-covered area of the lenses were little affected in comparison with the results found with single-vision lenses.[4] Both MiyoSmart and Stellest lenses have been shown to produce a significant reduction in myopia progression after 2 years of MS lens wear in comparison to single vision lens wear.[4, 5, 16, 21]

These two variants of MS-type lenses are now becoming available for clinical use in several parts of the world. Other variants may follow. Clinicians and researchers need to understand the design and optical characteristics of the lenses, not least to enable them to

check the lenses in their labs before dispensing to patients. This paper aims to describe the optical design and measured characteristics of available MS-type lenses.

Optical design: Geometrical Optics considerations

Hoya MiyoSmart spectacle lens

The original key concepts for any MS spectacle lens were, first, that at any part of the lens traversed by an image-forming pencil of rays from an object point in part or all of the peripheral field, there must be two focal powers, corrective and defocus, within the area corresponding to that of the entrance pupil of the eye. The second requirement was that the ratio of the areas occupied by these two powers within the pupil should remain reasonably stable as the pupil diameter changes or the eye moves. The MiyoSmart design of Fig.1a meets these requirements, its optical effects being shown schematically in Figure 2.

The carrier has a power which corrects the distance refractive error of the wearer. The lenslet size (1 mm diameter) and the centre-to-centre intervals between nearest neighbours (1.5 mm) are chosen to assure that, within any fixed circular pupillary diameter and at any part of lens, a reasonably stable number of lenslets is included within the pupil area and that the total area of included lenslets takes up approximately half that of the full pupil. In the MiyoSmart the lenslets occupy about 40% of the entire lenslet-covered area of the lens, although within any small pupil the proportion varies somewhat with the size and location of the pupil. Lenslet diameters <1.0 mm are unsuitable, due to the associated increase in image blur due to diffraction.

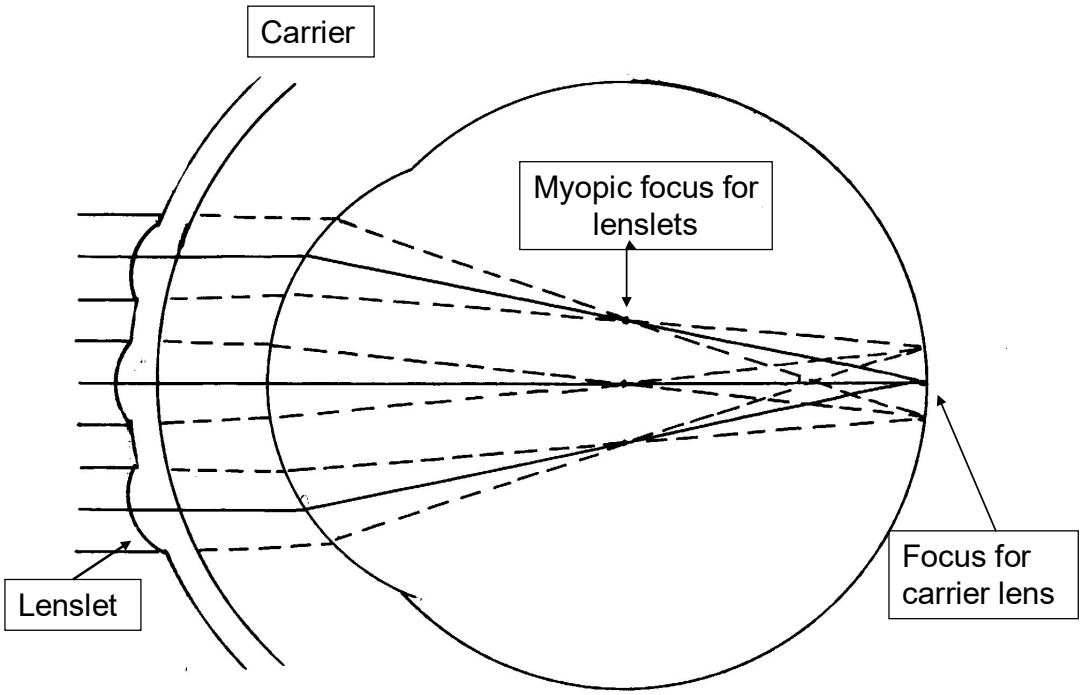

(a)

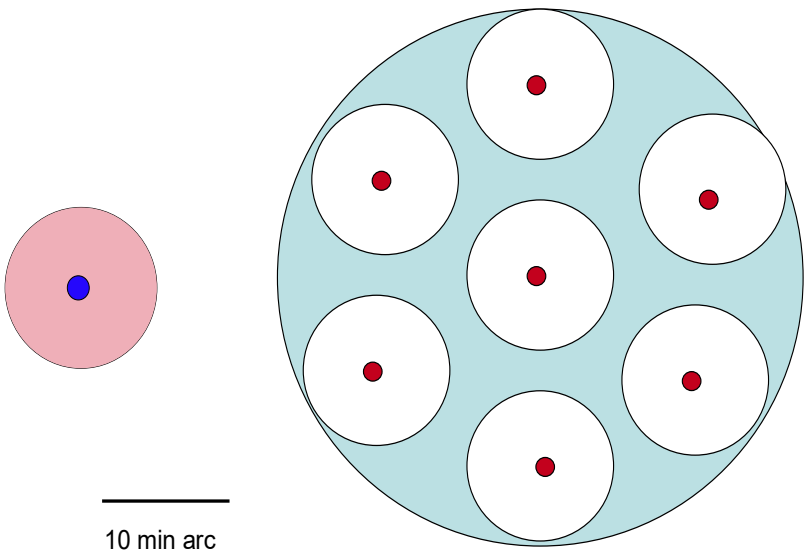

(b)

Figure 2. Schematic diagram (not to scale) showing (a) action of MiyoSmart *lens and eye when imaging a distant object point. The continuous rays are the chief rays for each*

lenslet, which pass undeviated through the optical centres of the lenslets to converge at the focus for the carrier lens on the retina. Other rays (shown dashed) passing through each lenslet are deviated to a myopic focus in front of the retina, the focus for each lenslet being laterally separated from those for its neighbours. For clarity, only 3 lenslets are shown. In practice the lenslets are confined to the outer portion of the lens, the central area being clear (see Figure1a). (b) MiyoSmart (DIMS) images of a distant object point according to geometrical optics in a reduced eye with a 4 mm diameter pupil. It is assumed that the lenslets are symmetrically distributed within the pupil, although in practice the distribution will change dynamically as fixation and the pupil diameter vary. (Left) On the retina, the base power of the carrier forms a point image (dark blue) and the lenslets generate a superimposed circular blur patch (pink). (Right) In the myopic plane of focus produced by the lenslets, each lenslet forms its own point image (red), these being laterally displaced from one another, and the carrier power creates a blur patch (pale blue) with a circular boundary.

The optical path according to geometrical optics of a ray pencil from a distant object through a basic MiyoSmart lens is shown schematically in Fig. 2a. As also discussed by other authors,[14, 15] in the absence of the lenslets, rays passing through the carrier to enter the eye's entrance pupil would all come to a focus on the retina. In any other transverse plane a uniform blur circle would be formed, with a diameter dependent on the pupil diameter and error in focus. However, in the presence of the lenslets, although the chief rays passing through the optical centres of the lenslets still all converge to the carrier's point focus, the other rays passing through each positively-powered lenslet are converged to a more anterior point focus positioned on the chief ray. Thus, in the myopic image plane corresponding to the lenslets' defocus power, the image consists of an array of point foci which are laterally distributed in the same spatial pattern as that of the lenslets within the pupil area. These images are superimposed on the blur patch due to the carrier power, which has a form which is a blur circle with circular dark areas corresponding to the areas of the lenslets. At the retina the carrier lens continues to create a point focus, but the ray bundle from each lenslet is now out-of-focus and creates a blur circle with a diameter which depends upon the diameter and power of the lenslet. Since the chief rays from the lenslets all converge at the retina, the individual lenslet blur circles are all superimposed on each other (Figure 2, see also Jaskulski et al.[14] and Gantes-Nunez et al.[15]).

If the minor effects of the vertex distance of the spectacle lens are neglected, it is straightforward to calculate the approximate angular scale of these point images. Using a reduced eye model of dioptric length *K"* dioptres, with a single refracting surface, if a circular pupil of diameter *D* is placed at this surface, the diameter of the retinal blur circle, *d,* for a simple spherical error of focus *ΔF* is:

$d = \Delta F.D/K'$

Taking a conventional reduced eye model with *K"* = 60 dioptres[22] if *ΔF* is in dioptres and *D* in mm, this corresponds to an angular diameter

$Ø = 3.44\ \Delta F.D$ min arc

Considering now the image on the retina, the carrier lens (base power) gives a sharp focus but the images produced by the 1 mm diameter lenslets are each 3.5 D out-of-focus (Fig 2b, left). All their superimposed circular blur patches therefore have a diameter of about 12 min arc. This defocused light primarily acts to reduce the contrast of the combined image: this modest reduction in image contrast would be expected to have little effect on high-contrast letter acuity.[23] In the focal plane corresponding to the focus for the lenslets, the circular boundary of the blur patch due to the carrier for an eye-pupil diameter of 4 mm is about 48 min arc. Each lenslet forms a sharp point focus, the individual point foci being separated laterally by about 18 min arc (Figure2b, right). This separation is easily resolvable at the fovea of the eye, so that the image of an extended object appears to be blurred and of reduced contrast. The number of lenslets contributing to the image will increase with any dilation of the ocular entrance pupil, and the exact spatial distribution of lenslets sampled will vary with changes in the direction of the visual axis and the field angle on the retina. In some cases, only part of a lenslet may fall within the pupil boundary, so that at the myopic focus not all of the component lenslet images are of equal retinal illuminance. The modulation transfer function will therefore vary with both time and orientation.

In practice these simple geometrical predictions are, of course, modified by such factors as the vertex distance of the MS lens, the changes in shape of the lenslet pattern and entrance pupil of the eye when viewed obliquely, diffraction, and the oblique astigmatism and other aberrations of the carrier lens and eye.

The effects of diffraction associated with the small diameter of the lenslets are particularly important. The 1.0 mm diameter of each lenslet acts in a similar way to that of the pinhole in the pinhole test: It increases diffractive blur and the depth-of-focus. In the absence of

any aberration and with monochromatic light of wavelength 555 nm, the in-focus point image (the Airy disc) has a diameter of about 4.6 min arc and the modulation transfer function falls to zero at a spatial frequency of about 31 c/deg. Thus, at best, the in-focus point-image formed by each lenslet is of relatively low optical quality. In practice, the images will be further degraded by additional aberrations. The small diameter of the lenses will also affect the out-of-focus characteristics of the lenslet images, and the associated depth-of-focus. If we apply the Rayleigh quarter-wavelength criterion of defocus, a defocus of about 1.1 D from the optimal focus is required before any additional image blur becomes detectable: experimental studies using various methods give similar values.[22] The poor sensitivity to focus change would be expected to make images formed by individual lenslets poor accommodation stimuli.[24]

The oblique astigmatism of the eye also has major impact on the blur patterns on the peripheral retina when the visual axis is directed through the lens centre. The typical oblique astigmatism of the eye rises from about 1 D at a field angle of 20 degrees to around 2.5 D at 40 degrees,[25] introducing corresponding additional spherical and cylindrical blur. Nevertheless, Figure2b would be expected to give a reasonable prediction of the general features of the images. We have confirmed this by ray-tracing with a Navarro model eye.[26] Examples of modulation transfer functions for various pupil diameters are available in literature.[14, 15, 18]

As manufactured, the MiyoSmart's lenslets are distributed across an approximately annular area of the carrier lens, with inner and outer diameters of 9.4 and 33 mm (in fact the boundaries are hexagonal). This region is centred on the optical centre of the carrier lens. This means that, with a properly-fitted lens and a vertex distance of 13 mm the angular radii of boundaries of the lenslet-covered area are about 16 and 45 degrees respectively when the spectacle lens axis and visual axis coincide. Under such circumstances, the lens acts as a single-vision distance correction with no loss of contrast for foveal vision, while the peripheral retina receives point images of the type illustrated in Figure 2. Changes in fixation direction with respect to the lens axis obviously change this situation, but, given that eye movements rarely exceed 20 degrees,[27] for most of the time the task of interest will be fixated through the clear area of the lens. Thus, accommodation is also usually governed by vision through this single-vision, distance-corrected area. If the visual axis is directed through the lenslet-covered areas of the lens, accommodation is still governed by the distance-corrected carrier image, since the multiple displaced images

formed by the lenslets at the myopic defocus form a confused, low-contrast image of any near stimulus.

The distortions and visual field with any MS lens are the same as with an equivalent single-vision lens without defocus lenslets. It is important for a child to form his/her space perception properly in the period when the visual system is still under development. Except for MS lenses, all spectacle-lens treatments (progressive, aspheric, bifocal) produce some undesirable distortion or field jump.

Essilor Stellest Lens

The broad features of this lens follow those illustrated schematically in Figure1b. There are 11 circular rings of lenslets, all concentric to the optical centre of the carrier lens, these cover all the lens blank except its central area, although when glazed in a spectacle frame some of the outer rings of lenslets may be wholly or partially missing. The clear area over the circular central part of the lens is about 9 mm in diameter, so that if gaze is directed through the centre of the area, all the lenslets lie at field angles greater than about 16 degrees. According to the manufacturers, each lenslet has a diameter of 1.12 mm and an aspherical rather than a spherical air-polycarbonate surface, with the design aim of replacing the single plane of myopic focus, as found in the MiyoSmart lenses, by an axially distributed focus (as in aspheric presbyopic contact lenses). This is achieved through the negative spherical aberration created by the aspheric surface. Two levels of aspherisation have so far been used – slightly aspheric lenses (SALs) and highly aspheric lenses (HALs) – although commercial lenses are now HALs. According to Li et al.[18] the SALs have a range of myopic foci lying 1.0 to 1.3mm anterior to the retina and the HALs between 1.1 and 1.9mm. Approximate calculations suggest that, under these conditions, the range of myopic errors of focus for each SAL is about +2.8 to + 3.7 D and that for each HAL is about +3.1 to +5.6 D. As yet, however, no details have been published of the exact radial power gradients of the aspheric lenslets.[15] The limited information currently available suggests that the relative positions of the lenslet foci with respect to the retina are maintained across the retina, implying that the powers of consecutive circles of lenslets are systematically varied with the radius of the lenslet ring to allow for the effect of the peripheral refraction of the eye. Bao et al.[16] state "*The calculations for the lenslets were based on the modified Atchison eye model[28] using a retinal shape modified to match the peripheral refraction data of Chinese children.[29-31]*" Note that allowance for the effects of the typically hyperopic relative peripheral refractive error (RPRE) will only be effective if

the child looks through the centre of the carrier lens and has the “average” RPRE. Presumably only the mean spherical component, *M,* of the RPRE is allowed for, the cylindrical vector components J_{180} and J_{45}[32] remaining uncorrected. Similarly, known differences between the RPRE in different meridians of the eye and variations with the magnitude of the myopia[33] must be ignored.

Point images in various planes can be derived in principle, as for the MiyoSmart lenses. The aspheric form of the lenslets would be expected to reduce the image quality at their optimal focus but to extend the focal range over which reasonable image quality is achieved. As in the MiyoSmart case (see Figure2), the spatial distribution of the lenslet images in any plane of focus away from the carrier focus will correspond with that of the lenslets in relation to the pupil area. Since the lenslets are arranged in concentric rings, for any constant pupillary area the pattern of lenslets within the pupil will change according to the pupil geometry and the area of the lens traversed by the imaging pencil of rays. Representative modulation transfer functions for the lenses, which vary with pupil diameter and position and grating orientation, have been presented by Li et al[18] and Gantes-Nunez et al.[15]

Objective evaluation of the optical properties

Methods

It is important to establish that it is possible to verify whether any MS lens as manufactured match the design specification. Three techniques were used: surface images, Twyman-Green interferometry and focimetry. Tests were applied to 2-4 lenses of different base powers for each lens type.

Surface images: Under normal ambient indoor or outdoor conditions, it is very difficult to detect the lenslets on either the MiyoSmart or Stellest lens surface. However, the surface relief can be revealed by using suitable directional oblique illumination and recorded with a macro camera. A scale was photographed under the same conditions to allow dimensional information to be obtained.

Twyman-Green Interferometry: A modified custom built two-beam Twyman-Green interferometer[25, 34] was used to check the curvature and asphericity of the surface of the

carrier and its lenslets, the lens being placed in one beam, with air in the other. Points lying on neighboring black fringes of the resultant interferograms differ by a half-wavelength of optical path. An expanded beam from a HeNe laser (wavelength 633 nm) was used for illumination and digital interferometer images were recorded through various regions of the MS lenses.

Since the optical path difference with respect to air is $(n\text{-}1)t$, where n is the refractive index of the lens and t is the physical distance through the lens, it is possible to estimate the centre thickness and surface form of the lenslets. Unfortunately, the $(\cos\theta)^2$ intensity variation of the broad two-beam fringes of the Twyman Green interferometer (θ being the angular phase difference between the beams) limits the accuracy with which the diameters of the annular bright or dark fringes corresponding to the lenslets can be estimated. However, approximate values can be obtained. These can then be compared with those expected on the assumption that the lenslet has a single spherical surface.

Strictly speaking, the lenslets are of meniscus form since their rear surfaces are effectively in contact with the convex anterior surface of the carrier lens. The calculations, however, are carried out more simply if the assumption is made that the lenslets are of the same power but have a plano-spherical form, since this involves a bending of the lens which does not alter the spatial variation in optical thickness across the lens.

With these limitations, a contour map for optical path difference (OPD) variations across the lens can be constructed. If a dark fringe (or spot) is located at the centre of a lenslet, the surrounding annular bright fringe represents a contour corresponding to a difference in OPD with respect to the lens centre of a quarter-wavelength, the next dark fringe to an OPD difference of a half-wavelength with respect to the centre, and so on. Hence if the diameters of each annular ring are measured, a contour map or section of the lenslet in terms of its OPDs can be generated. This, in turn allows the form of the lens surface to be determined for comparison with that expected for the specified lenslet form and power. This is done in terms of the sag across the convex surface as a function of zonal radius.

Focimetry: Conventional focimetry (Topcon LM-8C, Topcon, Topcon Healthcare - Seeing Eye Health Differently) was used to measure the carrier lens power and combined carrier-lenslet power, using a 7 mm diameter stop. Since the spatial distribution of the lenslets and their powers may vary across a Stellest lens,[16] a projection focimeter (Nikon PL-22, Nikon,

Nikon) with its stop diameter reduced to 1.5 mm was used to explore these aspects in more detail. Lenses were traversed across the focimeter stop in a direction perpendicular to the focimeter axis so that powers could be measured at 0.5 mm intervals along a lens diameter. When the lens was traversed across the 1.5 mm diameter stop, the focimeter beam often sampled both the lenslet and base power areas of the lens, in which case the power derived from the brighter of the two images was recorded. Although the lenslets had aspherical surfaces, no difficulty was found in locating the corresponding optimal focimeter images. Three measurements were made at each lens position and the measurements were repeated with the traverse direction reversed. All results were averaged. Since the back surface of the Stellest lenses had a radius of curvature of about 81.5 mm, the back vertex distance varied as the lens was traversed over the focimeter stop. All powers were therefore corrected to a vertex distance of zero.

Results

MiyoSmart lenses

A typical surface image is shown in Figure 3. Measurements of various lenses at different magnification levels confirmed the expected regular triangular spatial arrangement of the lenslets. Their diameters and centre-to-centre separations were measured as 1.00 ± 0.04 and 1.51 ±0.03 mm respectively, close to the nominal values of 1.0 and 1.5 mm.

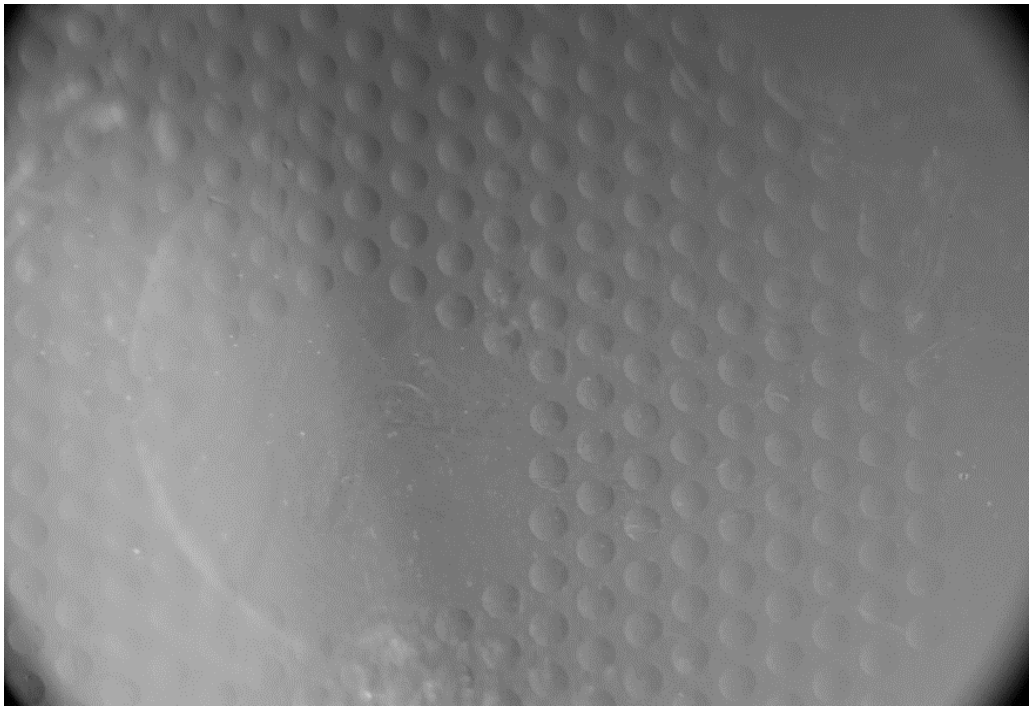

Figure 3. Anterior surface of a MiyoSmart lens, showing the triangular array of lenslets, together with part of the central clear area of the carrier lens. The lenslet spacing is 1.5 mm.

Figure 4 shows a typical MiyoSmart Interferogram. The optical centre of the afocal carrier lens is above the recorded area. Note that fringes from the individual circular lenslets can be seen against a broad ring pattern due to the carrier lens. There are about 1.5 fringes between the centre and edge of each lenslet and, as in Figure 3 there are no obvious irregularities in either their shape or spacing.

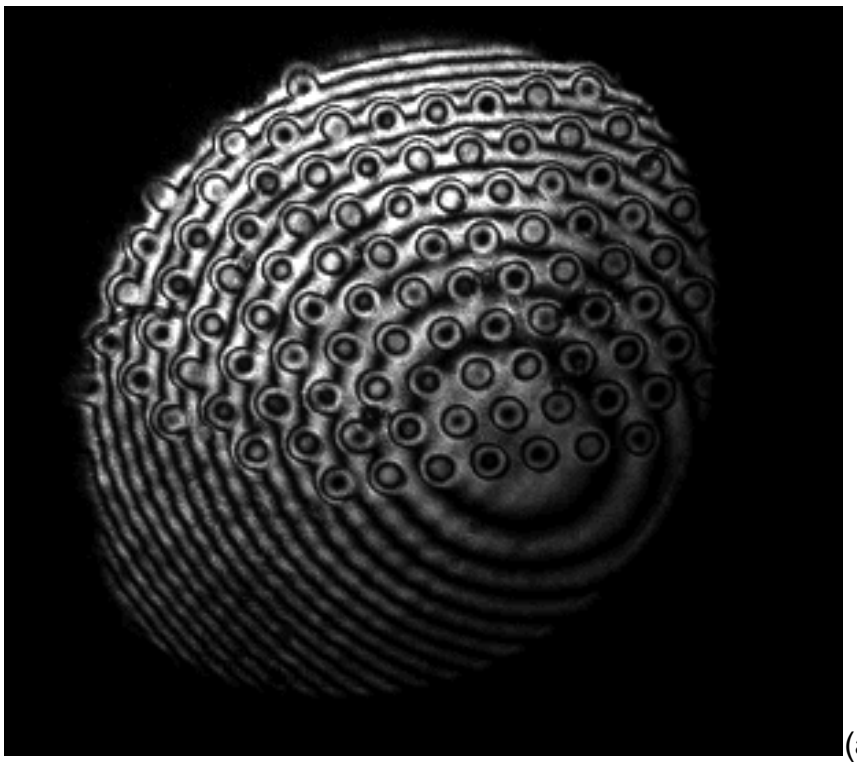

(a)

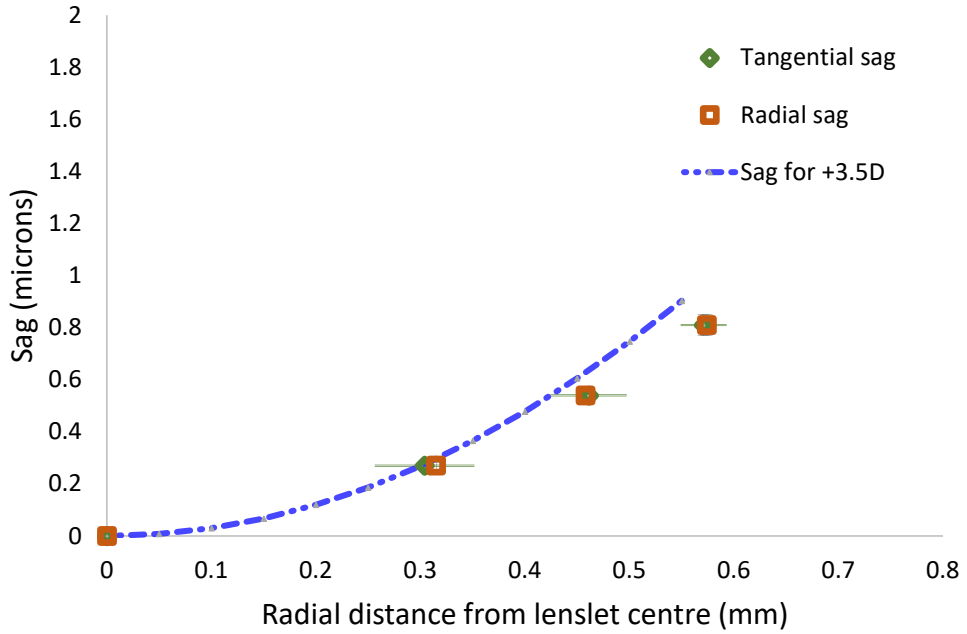

(b)

Figure 4. (a) An example of the Twyman-Green interferometer images of an afocal MiyoSmart lens. Inter-lenslet distances are all 1.5 mm. The optical centre of the lens is above the illustrated area. (b) Sag of the anterior surface of a lenslet in equivalent plano-convex form as a function of the radial distance from its centre. The continuous curve is derived from the assumption that the lens has power 3.5 D and refractive index 1.586, giving a radius of curvature for the air-polycarbonate surface of 167 mm. The red and green data points are estimates from the interferograms. across lenslet diameters oriented in directions which are tangential or radial with respect to the optical centre of the carrier lens. Standard deviations are based on measurements of 10 lenslets.

We can now check whether the lenslets have a form appropriate to their powers. As noted earlier, although the lenslets are in fact meniscus in form, with their back surface curvature matching that of the carrier lens, we can treat their optical thickness as varying in the same way across the lens as in a plano-convex lens of the same power. Calculation shows that a plano -convex lenslet with a power of +3.5 D and diameter 1.0 mm fabricated in polycarbonate of refractive index 1.586 should have an anterior radius of curvature of 167 mm and a centre thickness of about 0.75 microns. The expected difference in optical path between light which traverses this thickness of polycarbonate and the corresponding distance in air is 0.44 microns, equivalent to about 1.4 complete fringes at the 633 nm laser wavelength. For example, if the interferogram for a lenslet had a black fringe at the

centre, it should be surrounded by one bright and one dark circular fringe with a slightly brighter fringe round the perimeter. Figure 4b shows the results of such an analysis, based on 10 lenslets from different areas of the lens. There is reasonable agreement between the predicted and observed results. The outermost data point, which lies outside the nominal radius of the lenslet, is unreliable due to the deformation of the interference fringes at the surface discontinuity. Analysis of the broad background fringes due to the carrier lens suggests a power of 0.05 D for the nominally afocal carrier. The non-zero measured power is attributed to the curved form of the afocal carrier lens and to small tilts in its orientation during the measurement process.

Figure 5 shows the focimeter images obtained from a region of a MiyoSmart lens with a nominal carrier power of -1.75D and lenslets of power +3.5D. No problems were encountered in obtaining mire images, the standard deviation of power settings typically being about 0.05 D and 0.08 D for the carrier lens and lenslets respectively. The focimeter image at a focus corresponding to the carrier power is seen in Figure 5a. The image from the lenslets is shown in Figure 6b. As expected, in Figure 5a the mire image corresponding at -1.75 D is sharp but some out-of-focus blur from the lenslets is visible. In contrast, in Figure 5b, a focimeter setting of + 1.75 D. corresponding to the power of each segment in combination with the carrier lens again gives an in-focus image of the circle of dots forming the focimeter mire, but the centres of the mire images corresponding to the different lenslets falling within the 7 mm focimeter aperture are displaced to form a triangular array due to the spatial arrangement of the lenslets. The mire circles overlap to produce brighter dots at their intersection points. There is weak out-of-focus background blur from the carrier lens. Evidently, the characteristics of the mire images are in general agreement with the predictions of Figure 2. Overall, the optical characteristics of this and other, MiyoSmart lenses appear to match their specification.

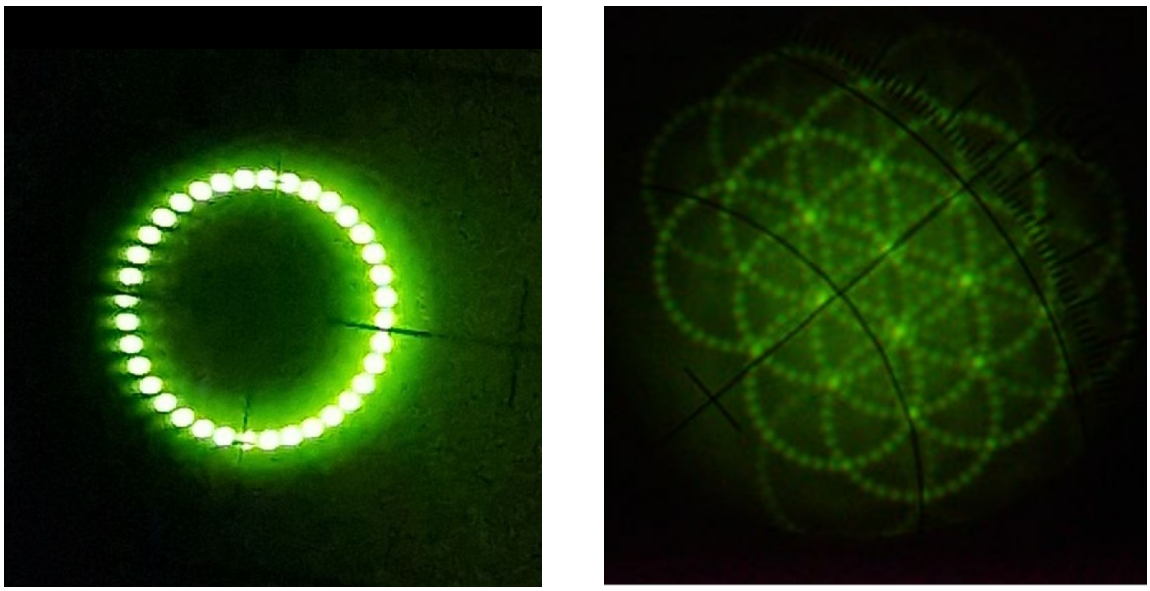

(a) (b)

Figure 5. Images of the focimeter mire with a MiyoSmart lens and focus settings for (a) the carrier lens and (b) the lenslets . The focimeter stop diameter was 7.0 mm, sufficient to include several lenslets. Note that the magnification of the illustrated carrier image is 1.6 X larger than that for the lenslet images. In practice, the size of the image formed by each lenslet is the same as that formed by the carrier lens.

Stellest lenses

The same assessment methods were applied to current commercial Stellest lenses, which appear to be of the HAL design.

Surface imagery suggested that the basic configuration of the lenslets was in accord with published information (Figure 6) Note the close centre-to-centre spacing of the lenses along the perimeter of each ring (about 1.21±0.02 mm) and the much wider spacing between neighbouring rings (2.51±0.05 mm). These orientation-dependent spacings cause the pattern of lenslets across the eye's pupil to vary substantially with the gaze direction.

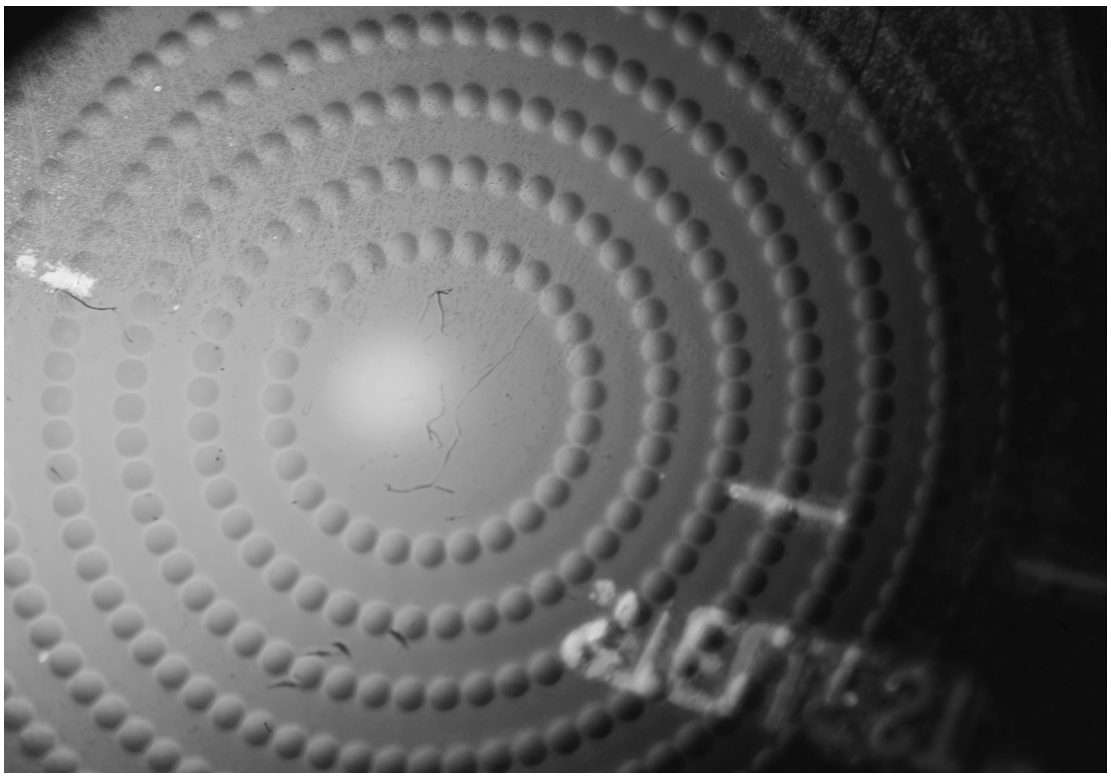

Figure 6. Surface reflection image of central region of a Stellest spectacle lens, with its concentric circles of lenslets. Successive lenslet rings differ by 2.5 mm in radius.

Twyman-Green two-beam interferometry again shows the concentric circles of lenslets superimposed on the smooth carrier lens (Figure7a). Analysis of the fringe patterns for individual lenslets suggests that the close spacing of the lenslets around each ring results in the effective diameter of each lenslet being smaller in the tangential direction around the ring than in the radial direction towards the ring centre, i.e. the rotationally-symmetric lenslets are slightly truncated. Further, there is evidence that, as stated by the manufacturers, the lenses are markedly aspheric, with the surface curvature reducing towards the lens periphery (Figure 7b). The overall radius of the lenslets in the meridian oriented towards the optical centre of the carrier appears to be larger (at about 0.7 mm, see, Figure 7b) than the value of 0.56 mm quoted by the manufacturers.

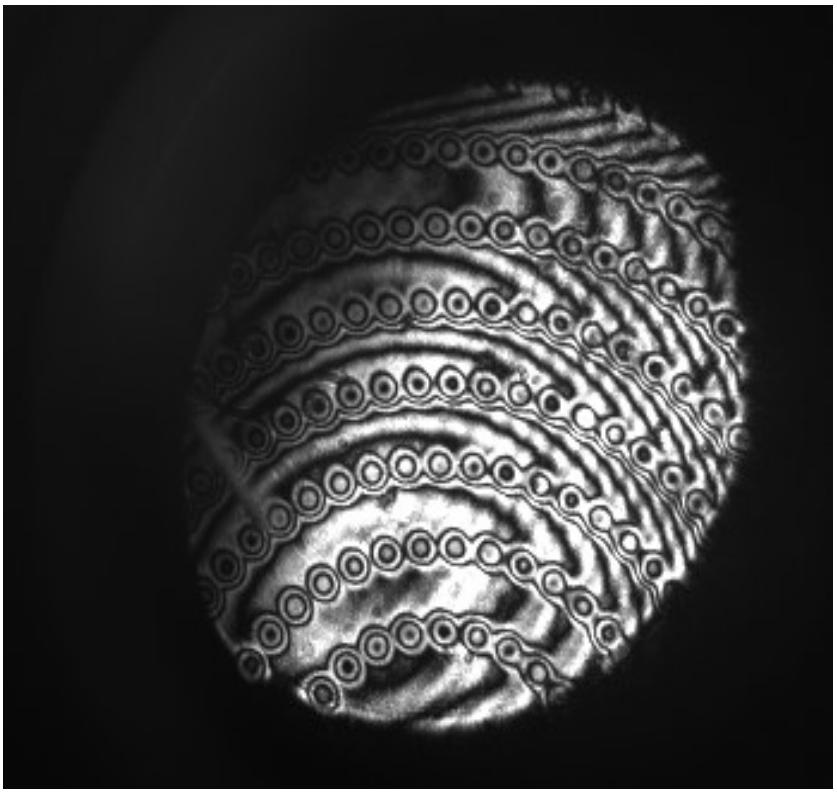

(a)

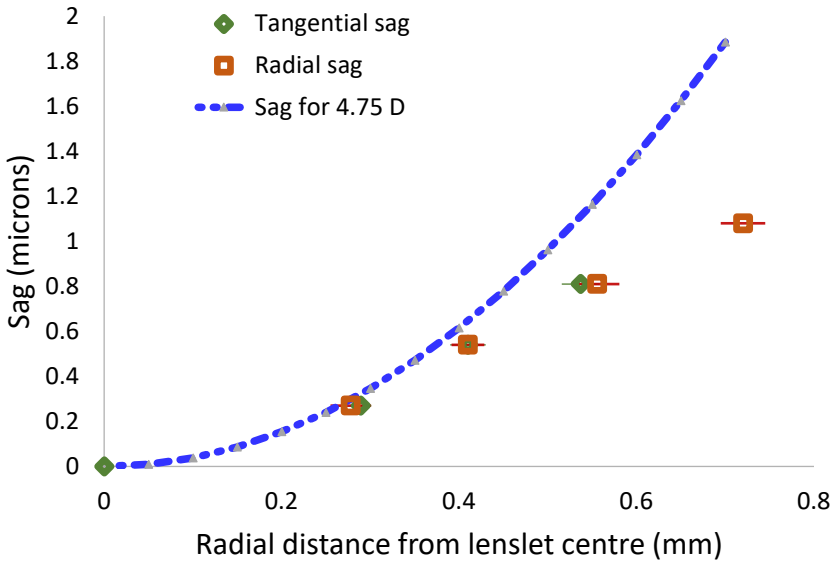

(b)

Figure 7. (a) Twyman-Green interferogram of afocal Stellest lens, showing the 7 central rings of lenslets. (b) Radial variation in the sag across the la diameter of a lenslet surface. The smooth curve corresponds to the sag expected for a +4.5 D lenslet with a spherical surface and the red and green symbols show data along Stellest lenslet radii oriented tangentially and radially with respect to the centre of the carrier lens.

With the Topcon focimeter, clear mire images were obtained in the expected 2 focal planes, with the spatial structure of the lenslet mire image being related to the distribution of lenslets within the focimeter aperture (Figure 8). Local measurements at suitable points across lenses of different base powers with the Topcon instrument confirmed that the base powers were correct. Repeated measurements of the powers of individual lenslets in the periphery (radial distance from the centre 12 mm), using the Nikon instrument with a 1.5 mm stop, gave a value of 4.14 ± 0.48 D.

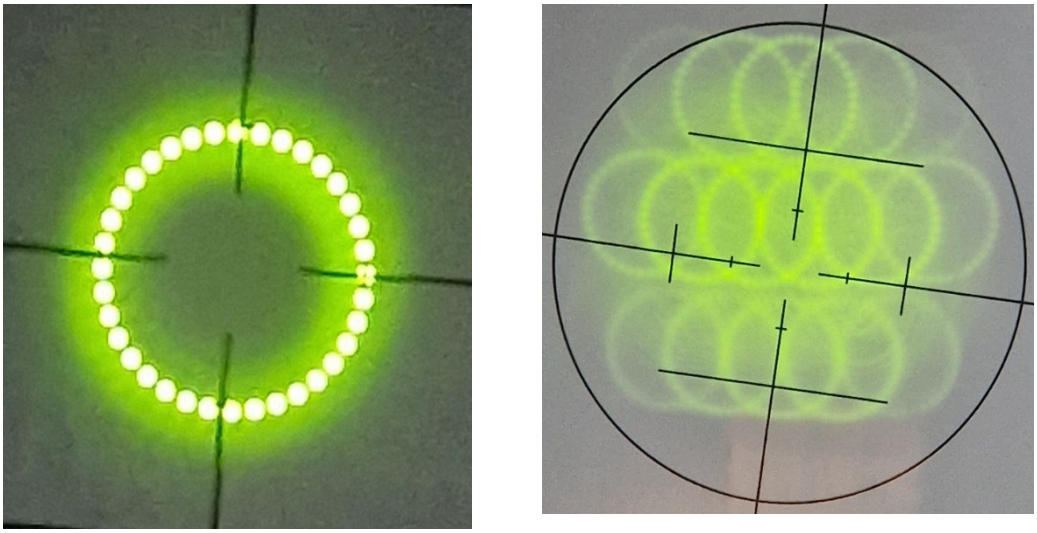

(a) *(b)*

Figure 8. Images of the focimeter mire with a Stellest lens and focus settings for (a) the carrier lens and (b) the lenslets. The focimeter stop diameter was 7.0 mm, sufficient to include parts of 3 circles of lenslets. Note that the magnification of the illustrated carrier image is 2.4 X larger than that for the lenslet images. In practice, the size of the mire image formed by each lenslet is the same as that formed by the carrier lens.

The results of power measurements using a small focimeter stop along a radius of an afocal Stellest lens are shown in Figure 9. As expected, the power values oscillate between the carrier power of 0.00 D and a lenslet power of approximately 4.25 D, with a period corresponding to a difference of 2.5 mm between the radii of successive lenslet rings. The irregularities in the spatial periodicity of the measurements can reasonably be

attributed mainly to the coarse sampling frequency of the measurements (0.5 mm), and the fact that lenslets in successive rings are not necessarily centred along all diameters of the carrier lens.

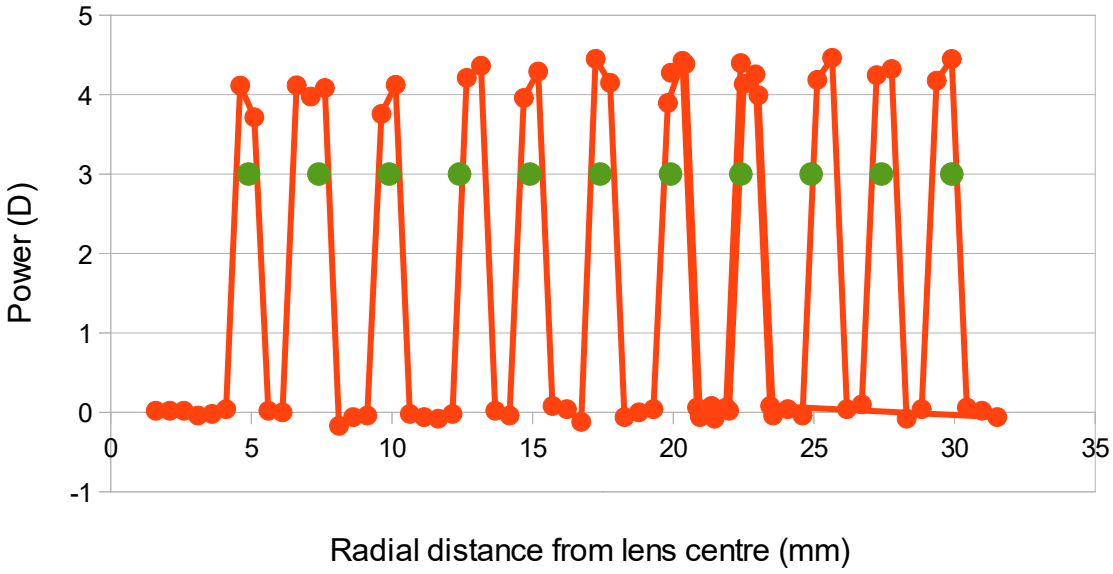

Figure 9. Focimeter measurements at 0.5 mm intervals of the power of a plano Stellest lens in a radial direction from the carrier lens centre. Power values have been corrected to zero back vertex distance. The green symbols give the expected radii of the 11 rings of lenslets, based on the assumption that successive rings differ in radius by 2.5 mm.

Discussion

The present work confirms that the major optical characteristics of the MS lenses as fabricated broadly match their claimed specifications. It is possible to use clinically-available instruments such as focimeters to measure the powers of the lens and the segments (lenslets), enabling a clinician to monitor accuracy of dispensing with ease. In the central zones, the images obtained by the focimeter are similar to those obtained with single-vision lenses and elsewhere the focimeter images produced by the segments form a multiple image pattern, as shown in Figures 5 and 8. The surface images of the MS lens can be used to check for any surface errors and to ensure that the multiple segments are present.

The dimensions, spatial arrangement, powers and surface form (spherical) of the MiyoSmart lenslets were found to be as stated by the manufacturer. This was also true for the spatial distribution of the Stellest lenslets. However, the claimed characteristics of the Stellest lens differ from those of the MiyoSmart design in two important ways: the lenslets are “highly aspherical” and they vary systematically in power with the radius of the lenslet ring.[4, 16] The asphericity is intended to provide an extended focus than the single plane of myopic defocus generated by lenslets with a spherical surface. The interferometric data suggest that the lenslets are indeed aspherical, such that their zonal power decreases with distance from the lenslet centre, Unfortunately, limitations in the interferometric technique used prevented the characteristics of this asphericity from being defined precisely.

In relation to lenslet power variations, Bao et al[16] suggest that, in order that the images formed by the lenslets should maintain a constant position with respect to the retina across the lens, the lenslets are designed to vary in power with the lenslet ring diameter in a way that matches the typically hyperopic relative peripheral refractive error (RPRE) of the young myope. As can be seen from Figure 9, the recorded positive values increased slightly with distance from the lens centre, the power difference between the lenslets of the smallest and largest rings being about +0.36D. A regression line fit to the lenslet power data gave the equation

$F = 0.014x + 3.92$ ($R^2 = 0.31$)

where F is the lenslet power (D) and x is the ring radius (mm). The slope is significant at the $p<0.01$ level.

Qualitatively, this result appears to support Bao et al.' s statement.[16] However it must be remembered that, when the wearer's eye views through the lens centre, for the peripheral retina the chief rays which enter the eye after passing through the rings of lenslets may make considerable angles with the visual axis, i.e. they correspond to quite large field angles. The field angles which the incident chief rays must have on each ring in order to be refracted to pass through the pupil centre can be estimated by using the combination of a suitable schematic eye model with the geometry of the Stellest lens, particularly its back surface curvature and its vertex distance. We used a combination of a Lotmar schematic eye model[35] with a plano Stellest lens having a back surface radius of curvature of 81.5 mm as measured experimentally. The lens was placed at a back vertex distance of 12 mm

from the cornea. Figure10 shows the lenslet ring powers with respect to that of that of the smallest ring (i.e. $F_n - F_1$, where F_1 is the power of the smallest ring and F_n is that of the n th ring, so that $F_n - F_1$ is effectively the “correction” provided for the eye's own RPRE) plotted as a function of the resultant estimates of the field angles for the chief rays passing through each ring. This is compared with various experimental measurements of the RPRE of young myopes.[29, 31, 33] Although the measurements of RPRE have the same trend with field angle as the lenslet powers, in general the changes in lenslet power are substantially smaller than those required to balance the changes in RPRE. It therefore seems unlikely that the relatively small differences in power between successive rings of lenslets could play any major role in the ability of the Stellest lens to retard myopia development.

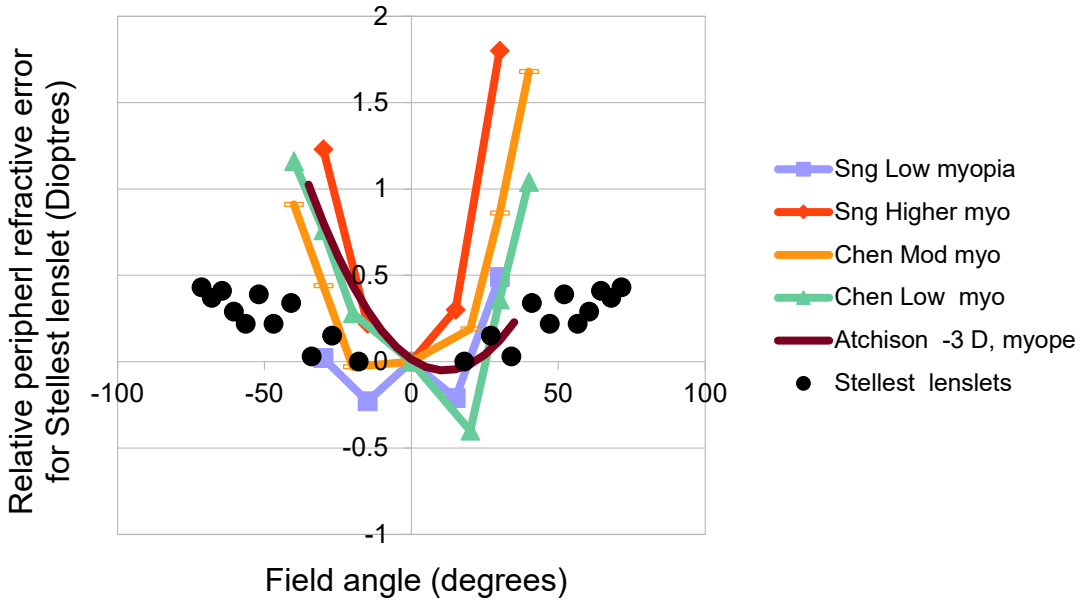

Figure 10. Possible compensation for the variation in the RPRE of myopes with field angle by the increase in the power of each ring of Stellest lenslets with lenslet ring radii. For the Stellest lenses (black symbols) the increase in the power of each lenslet ring above the smallest ring is plotted against the effective field angle of that ring when fixation is through the carrier lens centre. The other data are published mean results for the variation in RPRE with field angle.: Sng et al.[29] for Chinese children of mean age 7 years with either higher (M ≤-3 D) or lower (-3D < M ≤0.5D) levels of myopia; Chen et al.[31] for Chinese children aged 8-12 years, with either low (-0.50 D < M ≤ -3.00 D) or moderate (-3.00< M ≤-6 D) myopia; and Atchison et al.[33] for -3 D myopic adults.

Apart from the trial indicating that, with Stellest lenses, higher levels of lenslet asphericity give higher efficacy for the control, of myopia development,[16] no formal studies have been published on the clinical impact of changes in the parameters of MS lens designs. Further work is required to explore the way in which the powers, form and distribution of the MS lenslets affect the control achieved, so that optimal designs can evolve to be evaluated in clinical trials.

Conclusions

Current MS lenses are designed to produce both retinal and relatively myopic regions of focus in the mid-periphery of the wearer's visual field, using an array of small, circular, positively-powered lenslets on the anterior surface of a single-vision carrier lens which corrects the patient's refractive error. When viewing through a lenslet-covered area of the MS lens, the optical characteristics of the images in the two focal regions differ, that at the myopic focus containing multiple in-focus but laterally displaced images. Both carrier lens and lenslet powers can easily be measured with a focimeter. The optical quality of available manufactured MS lenses appears to approximately match that expected from the published design specifications.

Acknowledgements: This work was partially supported by PolyU grants ZVN1 and funding from InnoHK initiative and the Hong Kong Special Administrative Region Government to CSY Lam. We are grateful to Dr Michael Read for technical assistance.

Authors' Contribution statement:

H Radhakrishnan: Methodology; formal analysis; writing – original draft, review and editing. **CSY Lam:** Conceptualization; writing – review and editing. **WN Charman:** Conceptualization; formal analysis, Writing – original draft, review and editing.

References

1. Holden BA, Fricke TR, Wilson DA, Jong M, Naidoo KS, Sankaridurg P, et al. Global Prevalence of Myopia and High Myopia and Temporal Trends from 2000 through 2050. Ophthalmology. 2016;123(5):1036-42. Epub 20160211.
2. Bullimore MA, Brennan NA. Myopia Control: Why Each Diopter Matters. Optom Vis Sci. 2019;96(6):463-5.
3. Bullimore MA, Ritchey ER, Shah S, Leveziel N, Bourne RRA, Flitcroft DI. The Risks and Benefits of Myopia Control. Ophthalmology. 2021;128(11):1561-79. Epub 20210504.
4. Bao J, Huang Y, Li X, Yang A, Zhou F, Wu J, et al. Spectacle Lenses With Aspherical Lenslets for Myopia Control vs Single-Vision Spectacle Lenses: A Randomized Clinical Trial. JAMA Ophthalmol. 2022;140(5):472-8.
5. Lam CSY, Tang WC, Tse DY, Lee RPK, Chun RKM, Hasegawa K, et al. Defocus Incorporated Multiple Segments (DIMS) spectacle lenses slow myopia progression: a 2-year randomised clinical trial. Br J Ophthalmol. 2020;104(3):363-8. Epub 20190529.
6. Tabernero J, Vazquez D, Seidemann A, Uttenweiler D, Schaeffel F. Effects of myopic spectacle correction and radial refractive gradient spectacles on peripheral refraction. Vision Res. 2009;49(17):2176-86. Epub 20090613.
7. Sankaridurg P, Donovan L, Varnas S, Ho A, Chen X, Martinez A, et al. Spectacle lenses designed to reduce progression of myopia: 12-month results. Optom Vis Sci. 2010;87(9):631-41.
8. Liu Y, Wildsoet C. The effect of two-zone concentric bifocal spectacle lenses on refractive error development and eye growth in young chicks. Invest Ophthalmol Vis Sci. 2011;52(2):1078-86. Epub 20110222.
9. Liu Y, Wildsoet C. The effective add inherent in 2-zone negative lenses inhibits eye growth in myopic young chicks. Invest Ophthalmol Vis Sci. 2012;53(8):5085-93. Epub 20120731.
10. Smith EL, 3rd. Optical treatment strategies to slow myopia progression: effects of the visual extent of the optical treatment zone. Exp Eye Res. 2013;114:77-88. Epub 20130103.
11. Troilo D, Smith EL, 3rd, Nickla DL, Ashby R, Tkatchenko AV, Ostrin LA, et al. IMI - Report on Experimental Models of Emmetropization and Myopia. Invest Ophthalmol Vis Sci. 2019;60(3):M31-M88.
12. To CL, SY; Hatanaka, T; Masuda, Y, inventorSpectacle lens2019.
13. Lam CSY, Tang WC, Qi H, Radhakrishnan H, Hasegawa K, To CH, et al. Effect of Defocus Incorporated Multiple Segments Spectacle Lens Wear on Visual Function in Myopic Chinese Children. Transl Vis Sci Technol. 2020;9(9):11. Epub 20200805.
14. Jaskulski M, Singh NK, Bradley A, Kollbaum PS. Optical and imaging properties of a novel multi-segment spectacle lens designed to slow myopia progression. Ophthalmic Physiol Opt. 2020;40(5):549-56. Epub 20200818.
15. Gantes-Nunez J, Jaskulski M, Lopez-Gil N, Kollbaum PS. Optical characterisation of two novel myopia control spectacle lenses. Ophthalmic Physiol Opt. 2023;43(3):388-401. Epub 20230204.
16. Bao J, Yang A, Huang Y, Li X, Pan Y, Ding C, et al. One-year myopia control efficacy of spectacle lenses with aspherical lenslets. Br J Ophthalmol. 2022;106(8):1171-6. Epub 20210402.
17. Gao Y, Lim EW, Yang A, Drobe B, Bullimore MA. The impact of spectacle lenses for myopia control on visual functions. Ophthalmic Physiol Opt. 2021;41(6):1320-31. Epub 20210916.
18. Li X, Ding C, Li Y, Lim EW, Gao Y, Fermigier B, et al. Influence of Lenslet Configuration on Short-Term Visual Performance in Myopia Control Spectacle Lenses. Front Neurosci. 2021;15:667329. Epub 20210525.

19. Kaymak H, Neller K, Schutz S, Graff B, Sickenberger W, Langenbucher A, et al. Vision tests on spectacle lenses and contact lenses for optical myopia correction: a pilot study. BMJ Open Ophthalmol. 2022;7(1):e000971. Epub 20220405.
20. Lu Y, Lin Z, Wen L, Gao W, Pan L, Li X, et al. The Adaptation and Acceptance of Defocus Incorporated Multiple Segment Lens for Chinese Children. Am J Ophthalmol. 2020;211:207-16. Epub 20191213.
21. Lam CS, Tang WC, Lee PH, Zhang HY, Qi H, Hasegawa K, et al. Myopia control effect of defocus incorporated multiple segments (DIMS) spectacle lens in Chinese children: results of a 3-year follow-up study. Br J Ophthalmol. 2022;106(8):1110-4. Epub 20210317.
22. Atchison DS, G. Optics of the Human Eye. London: Butterworth-Heinemann; 2000.
23. Regan D, Neima D. Low-contrast letter charts as a test of visual function. Ophthalmology. 1983;90(10):1192-200.
24. Ward PA, Charman WN. On the use of small artificial pupils to open-loop the accommodation system. Ophthalmic Physiol Opt. 1987;7(2):191-3.
25. Radhakrishnan H, Charman WN. Optical characteristics of Alvarez variable-power spectacles. Ophthalmic Physiol Opt. 2017;37(3):284-96. Epub 20170217.
26. Navarro R, Santamaria J, Bescos J. Accommodation-dependent model of the human eye with aspherics. J Opt Soc Am A. 1985;2(8):1273-81.
27. Pynte J, Kennedy A. An influence over eye movements in reading exerted from beyond the level of the word: evidence from reading English and French. Vision Res. 2006;46(22):3786-801. Epub 20060830.
28. Atchison DA. Optical models for human myopic eyes. Vision Res. 2006;46(14):2236-50. Epub 20060221.
29. Sng CC, Lin XY, Gazzard G, Chang B, Dirani M, Chia A, et al. Peripheral refraction and refractive error in singapore chinese children. Invest Ophthalmol Vis Sci. 2011;52(2):1181-90. Epub 20110228.
30. Li SM, Wang N, Zhou Y, Li SY, Kang MT, Liu LR, et al. Paraxial Schematic Eye Models for 7- and 14-Year-Old Chinese Children. Invest Ophthalmol Vis Sci. 2015;56(6):3577-83.
31. Chen X, Sankaridurg P, Donovan L, Lin Z, Li L, Martinez A, et al. Characteristics of peripheral refractive errors of myopic and non-myopic Chinese eyes. Vision Res. 2010;50(1):31-5.
32. Thibos LN, Wheeler W, Horner D. Power vectors: an application of Fourier analysis to the description and statistical analysis of refractive error. Optom Vis Sci. 1997;74(6):367-75.
33. Atchison DA, Pritchard N, Schmid KL. Peripheral refraction along the horizontal and vertical visual fields in myopia. Vision Res. 2006;46(8-9):1450-8. Epub 20051213.
34. Kocher DG. Twyman-green interferometer to test large aperture optical systems. Appl Opt. 1972;11(8).
35. Lotmar W. A theoretical model for the eye of new-born infants. Albrecht Von Graefes Arch Klin Exp Ophthalmol. 1976;198(2):179-85.